

Excitonic trion population in two-dimensional halide perovskites

Efstratios Manousakis 

*Department of Physics, Florida State University, Tallahassee, Florida 32306-4350, USA
and Department of Physics, Harvard University, Cambridge, Massachusetts 02138, USA
and Department of Physics, National and Kapodistrian University of Athens, 157 84 Athens, Greece*



(Received 7 April 2024; revised 7 July 2024; accepted 2 August 2024; published 19 August 2024)

There are many reports of a surprisingly high charge-carrier density with sizable mobility in photoexcited two-dimensional (2D) halide perovskites despite their unusually high exciton binding energy. In this work we study the thermodynamic quasiequilibrium of the relative population of photoexcited free quasielectron/quasihole pairs, neutral excitons, and excitonic trions, in 2D materials that support such excitonic complexes with large binding energy. We derive and solve the general Saha equations which describe the detailed balance of such a system of photoexcited electronic degrees of freedom forming a multicomponent fluid of excitations in thermodynamic quasiequilibrium. The solution to these equations, for the special case of 2D perovskites where the reported exciton and excitonic trion binding energies are of the order of 0.3–0.4 eV for the former and 30–40 meV for the latter, reveals that while the charge-neutral excitonic population dominates all other excitations, at room temperature and below, the excitonic trion component can be the dominant population among charge carriers. We also argue that trionic hopping can take place via a tunneling mechanism which is speculated to play a role in a novel charge-transport mechanism.

DOI: [10.1103/PhysRevMaterials.8.084004](https://doi.org/10.1103/PhysRevMaterials.8.084004)

I. INTRODUCTION

Understanding the character and behavior of the charge and energy flow in semiconductor quantum wells can lead to efficient optoelectronic materials. In particular, the nearly ideal two-dimensional (2D) Ruddlesden-Popper perovskites are quantum wells which are self-assembled using wet-chemistry synthesis [1,2]. Their band gap is tunable, by varying the perovskite-layer thickness, and, thus, it can be used to modulate the effective electron-hole confinement. One of their unique features is the large exciton binding energy [3] which, depending on the type of superlattice structure, can reach values of several hundreds of meV. Analyzing the origin and the consequences of this feature should play a significant role towards an understanding of the nature of charge carriers and transport.

The reduced screening in such 2D materials enhances the Coulomb interaction and leads to tightly bound exciton and other excitonic complexes. For example, it has been experimentally shown [4] that in ultrathin layers of phenylethylammonium-lead-iodide [(PEA)₂PbI₄], the excitonic binding energy is approximately 0.35 eV. It is widely expected that light absorption creates excitons as long-lived excited states. As a result their optical absorption spectrum is dominated by an intense exciton peak below the band edge, with estimated binding energies of hundreds of meV. Therefore, in order to describe the equilibrium and nonequilibrium optical properties of 2D halide perovskites, first, we need to understand the role of strongly bound excitons.

However, while such a large exciton binding energy should hinder charge separation, there is significant evidence that there is an abundance of free carriers when the material is photoexcited. There are several attempts to explain such apparent

contradiction. One proposed explanation claims that the intragap edge states formed at the crystalline grain boundaries [5–8] play a key role in exciton dissociation. This proposed mechanism is related to the fact that solution-processed thin films are typically polycrystalline with grain boundaries featuring a high density of dangling bonds and defect edge states. The formation of polaronic excitons as well as polarons, where the carriers are strongly coupled to lattice deformations, are phenomena which seem to be established through various experimental probes [9–18] and they can play a significant role in resolving the appearance of charge carriers.

In the present paper we calculate the populations of the various components of the photoexcited quasiparticle/quasihole excitations, and, in addition, the neutral-excitonic and excitonic-trion population of the electronic system. We would like to point out that exciton relaxation dynamics has been recently studied by Ziegler *et al.* [4] in (PEA)₂PbI₄ where they demonstrate the emergence of both negatively and positively charged excitonic trions, with binding energies up to 46 meV, among the highest measured in 2D systems. They also demonstrate that trions dominate light emission and propagate with mobilities reaching 200 cm² V⁻¹ s⁻¹ at elevated temperatures. The goal of our present paper is to study the statistical mechanics of the quasiequilibrium of a multicomponent composite fluid of the above-mentioned long-lived photoexcitations in dynamic equilibrium with each other and with the gas of incident photons at a common temperature. We involve two energy scales in the problem: the large binding energy of an exciton which corresponds to several thousands of kelvin and a second energy scale which is the trion binding energy, which is an order of magnitude smaller and corresponds to hundreds of kelvin. We derive and solve the Saha equations for the composite fluid of these electronic excitations.

We show that, under a broad range of conditions, the trionic population at room temperature and below dominates the population of free quasielectron and quasihole carriers.

We also argue that these trionic charged excitations can move through the lattice under the influence of an external electric field via a novel quantum-mechanical tunneling mechanism of trions mediated by adjacent neutral excitons. This mechanism relies on the probability for a trion to be found next to a neutral exciton; however, this probability can become sizable at room temperature and below where the population of neutral excitons is maximum because of their large binding energy.

The paper is organized as follows. In the following section (Sec. II) we discuss the nature of the photogenerated excitations, i.e., quasiparticle/quasihole excitations and composite quasiparticles expected to be photocreated in 2D halide perovskites on general quantum many-body theoretical grounds. In Sec. III we present and solve the Saha equations for the more familiar case of neutral excitons in equilibrium with photoexcited electron/hole pairs (which may be influenced by strong polaronic effects). In Sec. IV we derive and solve the Saha equations for the more general case of a composite fluid of neutral excitons and positively and negatively charged excitonic trions in equilibrium with photoexcited quasielectron/hole pairs. In Sec. V we discuss our speculation of a trion-transport mechanism mediated by neutral excitons. Lastly, in Sec. VI we present our conclusions.

II. NATURE OF QUASIPARTICLES

There have been various attempts to demonstrate polaron formation in the 2D halide perovskites [9–17,19,20]. For example, using high-resolution resonant impulsive stimulated Raman spectroscopy [20], a vibrational wavepacket dynamics was identified that evolves along different configurational coordinates for distinct excitons and photocarriers. This observation [20] was interpreted as a signature of the polaronic character of excitons in two-dimensional lead halide perovskites, as different excitons induce specific lattice reorganizations. Furthermore, in Ref. [9] it has been convincingly argued that excitons, are in fact, exciton polarons, i.e., polaronic effects play a significant role in the formation of bound states of electrons and holes dressed with their cloud of lattice distortions. These effects are discussed in this section.

In addition, exciton relaxation dynamics has been recently studied [4] in (PEA)₂PbI₄ where the emergence of both negatively and positively charged excitonic trions, with binding energies up to 46 meV were discovered. Furthermore, it was found that excitonic trions dominate light emission and their mobilities reach 200 cm² V⁻¹ s⁻¹.

In this section, we first wish to clarify various concepts regarding the nature of elementary excitations in these 2D insulators in a manner consistent with quantum many-body theory. When we think about bands in materials, which are characteristic of the elementary excitations of the many-body system, we begin from the noninteracting electron represented by the bare propagator in Fig. 1. This describes a single electron moving in some form of periodic pseudopotential due to the presence of the ions and some additional average (exchange-correlation) effective potential

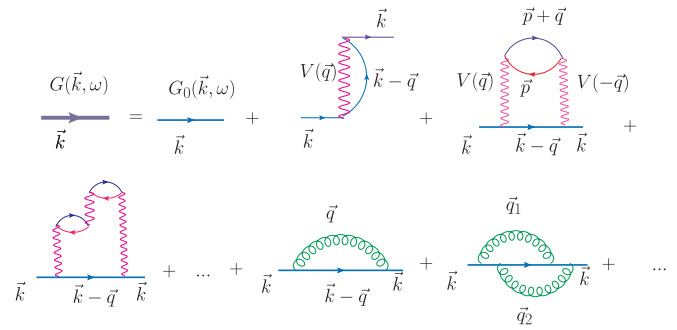


FIG. 1. The interacting Green's function of the quasiparticles (and quasiholes) which take into account the interaction with the other electrons of the Fermi sea and with the lattice. Its poles re-define the notion of the quasiparticle and quasihole to those which carry with them a cloud of virtual particle/hole excitations and a quantum gas of lattice virtual excitations (represented by the green wiggly lines, i.e., polaronic effects).

due to the spatially dependent density field generated by the collective presence of all the electrons. Such a picture can be best conceptualized within the Hohenberg-Kohn-Sham (HKS) density-functional-theory framework. Even though this is conceptualized as a free propagator, it includes the effects of the interactions with other electrons in a way that gives meaning to the single-particle picture. The HKS scheme is a purely ground-state theory. In order to study excitations above such a ground state we need to include the effects of correlations. These effects can be included perturbatively using the residual screened Coulomb electron-electron interaction. This interaction takes into account the effects of virtual particle/hole excitations due to the Coulomb interaction. In addition, allowing the ions to oscillate around their equilibrium positions, i.e., by including the lattice vibrations, leads to the quantization of their normal modes (phonons). The effects of the coupling of the electrons to these lattice excitations can be taken into account either perturbatively, as shown in the second line of Fig. 1 or nonperturbatively in the strong coupling limit, using some deformation potential approach. The series illustrated in Fig. 1 is written by means of the Dyson's equation for each band n as follows:

$$G_n(\vec{k}, \omega) = \frac{1}{\omega - e_n(\vec{k}) - \Sigma_n(\vec{k}, \omega)}, \quad (1)$$

where $e_n(\vec{k})$ is the energy of the n th noninteracting band and Σ is the so-called self-energy. The poles of this Green's function, assuming that the imaginary part of Σ becomes small as we approach the Fermi surface, are the quasiparticles, which define the renormalized bands. In the simplest picture, the ground state corresponds to filling these quasiparticle states with electrons up to the renormalized Fermi energy. Beginning from this new ground state one can carry out a perturbative scheme with these new quasiparticles defined on top of this Fermi sea and this scheme is repeated until self-consistency is achieved [21–24]. If this approach is met with no singularities and anomalies, we can say that the Fermi-liquid picture is valid and the band picture has a meaning.

Polarons are a fancy way of characterizing the renormalization of the quasielectrons and quasiholes which are also

dressed by the virtually excited phonons as shown by the green wiggly line of Fig. 1. Similarly, the electrons are dressed by the particle-hole excitations shown by those diagrams which contain the magenta wiggly interaction line of Fig. 1.

After taking into account such renormalization effects, it leads to lowering of the energy of single-particle states near the Fermi level. Namely, these effects define the nature of the free-quasiparticle states out of which the bands and the ground state are built.

These are the single quasiparticle and single quasihole states of this renormalized system of quasiparticles. Namely, elementary excitations which are created when a single electron or hole is added to the system. However, the photoexcitations created by the incident light are based on the simultaneous creation of quasielectron and quasihole excitations. Initially, the incident light perturbs the system and transfers energy to it. After a relatively short time of the order of 1–100 fs, the excited state of the electronic system can be described in terms of the following population of excitations. These excitations can be conceived as either free quasielectron/quasihole pairs (i.e., electrons or holes dressed with their ground-state polarization clouds and the cloud of lattice distortions or lattice vibrations as in Fig. 1) or bound states of these renormalized quasielectron/quasihole states.

Once a quasielectron (or polaron) is promoted from an occupied renormalized band to an unoccupied one, the Coulomb interaction acts between the created quasielectron and the created quasihole. This interaction is also renormalized by including the effects of screening, namely, terms involving the bubblelike diagram (Fig. 2) where quasiparticle/quasihole pairs are virtually created. These effects renormalize the bare Coulomb interaction by means of the dielectric matrix within the random-phase approximation (RPA) and some possible vertex corrections which go beyond RPA. In the case of the 2D halide perovskites, this interaction is also significantly affected by polaronic effects, which lead to a contribution to the residual interaction between quasiparticles (i.e., polarons) which can be also attractive due to the effect of lattice deformation. The leading perturbative term is shown in the top part of Fig. 2 as a phonon-exchange interaction between quasiparticles (green wiggly line). Once this interaction is constructed, we need to solve the Bethe-Salpeter equation (BSE), i.e., the problem of a quasielectron/quasihole pair on top of the interacting ground state (in the particle-hole channel) as illustrated in the bottom part of Fig. 2. We wish to emphasize that the quasiparticles entering the BSE can be strongly renormalized polarons. The solution to the BSE can lead to bound states between a polaronic quasielectron and a polaronic quasihole, which are excitons.

Next, we consider the effects of the coupling to phonons in an attempt to give a qualitative explanation of the results reported in Ref. [20], which were obtained by means of high-resolution resonant impulsive stimulated Raman spectroscopy. Let us just consider the effects of the diagram involving the green wiggly line in Fig. 2 to the effective electron-hole interaction, i.e.,

$$g_{\lambda}^2(\vec{k}, \vec{q}) \frac{\omega_{\lambda}^2(\vec{q})}{\omega^2 - [\omega_{\lambda}(\vec{q}) - i\eta]^2}, \quad (2)$$

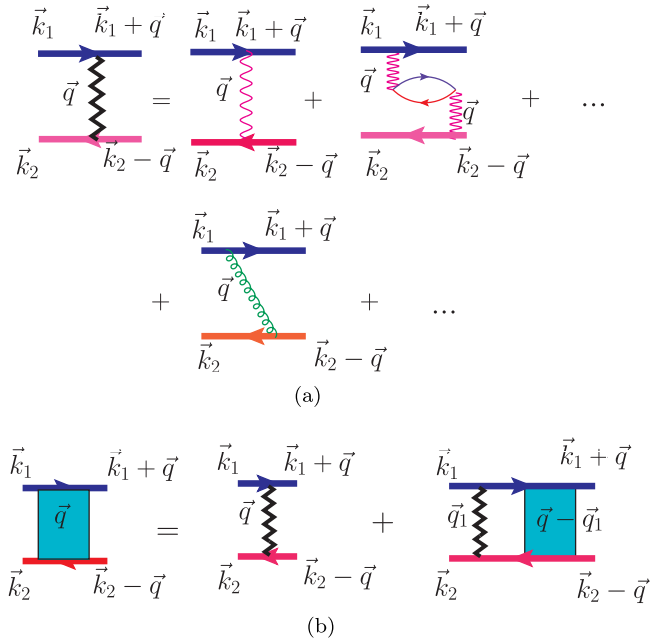


FIG. 2. (a) Renormalized quasiparticle interaction which takes the particle-hole polarization effects of the Fermi sea within the RPA (terms containing the particle/hole bubblelike diagram) and the phonon-mediated interaction (green wiggly line). (b) The Bethe-Salpeter equation for bound states between quasielectrons and quasiholes using the effective interaction defined in the top part of this figure. The cyan box is the full two-body vertex in the particle-hole channel.

where $g_{\lambda}(\vec{k}, \vec{q})$ is the electron-phonon coupling between a phonon mode λ of frequency $\omega_{\lambda}(\vec{q})$. By examining this expression, we expect to have a stronger resonant response in the excitonic spectrum at those phonon modes with the largest electron-phonon coupling and for energy transfer given by the phonon frequencies (we use units where $\hbar = 1$). While these experiments show that the electron is dressed by the lattice vibrations, they do not prove that a bound state between an electron and lattice deformation occurs. Moreover, the effect of the electron-phonon coupling may be taken into account perturbatively; namely, this effect just leads to a renormalization of the standard notion of the quasielectron carrying with it the distortion of the background ionic lattice. In fact, because we are dealing with fast dynamics and the lattice degrees of freedom respond with energy scales of the order of a few meV [20] (as expected on general grounds), we should see the dressing effects on the exciton after a timescale of a few picoseconds following the photoexcitation. Therefore, nothing really unexpected was revealed by these experimental findings suggesting that a dramatic nonperturbative effect between electrons and lattice distortions happens in these materials.

Is it possible that the single-polaron state, carrying with it a cloud of lattice deformations, as shown in Fig. 1, is a mobile boundstate to lattice distortions? Is it also possible that its bound-state energy is lower than the energy of the excitonic state? The answer is, in principle, yes to both questions. However, this would be an extraordinary effect and, while there is strong evidence for strong renormalization effects

on the electronic spectrum due to the virtual excitation of phonon modes [20], there is no smoking gun indicating such a nonperturbative effect.

These excitonic bound states can have structure as shown in Ref. [9], where the spectrum of these exciton-polaron states is discussed. As shown in Ref. [9], the center of the excitonic energy is a few hundreds of meV below the continuum of the free-carrier conduction band. In addition, there is a fine structure of various peaks separated by a much finer energy difference of the order of 30–40 meV. The center of these excitations, i.e., a scale of a few hundreds of meV, corresponds to the exciton binding energy while the fine structure corresponds to different types of excitons [9].

Now, once such excitonic bound states exist in the particle-hole channel, which are neutral excitations, we should ask if there are additional bound states, namely, charged excitations, which are bound states between an exciton and a quasiparticle. The reason for the possible existence of such excitations of bound states is the fact that an electric charge (that of the quasielectron or quasihole) and an electric dipole (that of the exciton) interact. In the formation of these *composite quasiparticles*, we expect the lattice to play a significant role, which means that polaronic effects are important to obtain an accurate quantitative description. Namely, they can be excitonic-polaronic trions dressed with strong lattice deformations. We discuss the nature of these bound states, denoted x^\pm , in the following section (Sec. IV). In addition, we may have biexciton bound states which are also strongly influenced by polaronic effects.

III. PHOTONS IN EQUILIBRIUM WITH EXCITONS, ELECTRONS, AND HOLES

When the incident photons are of energy greater than the 2D halide perovskite gap (of the order of 2 eV), they excite electrons from the valence band to the conduction band (which is filled with quasielectrons, i.e., electrons dressed with a cloud of lattice vibrations and, to a degree of lesser importance, a polarization cloud of virtual electrons and holes). After a timescale of the order of 20–100 fs, they form a population of free quasielectron (e^-) and quasihole (h^+) pairs (i.e., quasiparticles of strong polaronic character) in addition to excitons (x) and excitonic trions (x^\pm) of strong polaronic character. For simplicity, in the rest of this paper, we will refer to these quasiparticles of electron or hole character as simply electrons (using the symbol e^-), and holes (using the symbol h^+).

As a first step, we will ignore the presence of polaronic trions and we will deal with the familiar case of excitons and electron/hole distributions. Namely, we assume that every incident photon creates an electron/hole pair some of which bind (within a short timescale of the order of 10–100 fs) to form neutral excitons. After a thermalization timescale much shorter than the recombination timescale [25] we have photoexcited excitons (x) in quasiequilibrium with photoexcited electrons (e^-) and holes (h^+), i.e.,

$$x \longleftrightarrow e^- + h^+, \quad (3)$$

with relative area densities of excitons (n_x) and electron/hole pairs ($n_e = n_h$) satisfying the following constraint:

$$n_p = n_x + n_e, \quad (4)$$

where n_p is the incident photon density. In two dimensions we can describe this process by means of the so-called Saha equations [26,27]. Detailed balance leads to the following:

$$\begin{aligned} \frac{r_e r_h}{r_x} &= \frac{m_e k_B T}{\pi \hbar^2} e^{-E_b^0/k_B T}, \\ r_e &= \frac{n_e}{m_e^*}, \quad r_h = \frac{n_h}{m_h^*}, \quad r_x = \frac{n_x}{m_x^*}, \end{aligned} \quad (6)$$

where n_x , n_e , and n_h are the average density (number of particles per unit area) of excitons, electrons, and holes present in equilibrium ($n_e = n_h$). Here m_e^* , m_h^* , and m_x^* are the effective electron, hole, and exciton masses, respectively, in units of the bare electron mass m_e . The binding energy of the neutral exciton (x) is denoted above as E_b^0 .

We can rewrite these equations in units of the constant

$$\kappa_0 \equiv \frac{E_b^0 m_e}{\pi \hbar^2}, \quad (7)$$

which has dimensions of particle density, as

$$\frac{\rho_e \rho_h}{\rho_x} = \theta e^{-1/\theta}, \quad (8)$$

$$\rho_p = \rho_x m_x^* + \rho_e m_e^*, \quad (9)$$

$$\theta \equiv \frac{k_B T}{E_b^0}, \quad \rho_e = \frac{r_e}{\kappa_0}, \quad \rho_h = \frac{r_h}{\kappa_0}, \quad \rho_x = \frac{r_x}{\kappa_0}. \quad (10)$$

This set of equations leads to the following solution for the temperature dependence of the exciton and free-carrier fractions:

$$\rho_e = -\frac{\sigma_0(\theta) m_e^*}{2m_x^*} + \sqrt{\left(\frac{\sigma_0(\theta) m_e^*}{2m_x^*}\right)^2 + \sigma_0(\theta) \frac{\rho_p}{m_x^*}}, \quad (11)$$

$$\rho_x = \frac{\rho_e^2}{\sigma_0(\theta)}, \quad \sigma_0(\theta) \equiv \theta e^{-1/\theta}. \quad (12)$$

We note that σ_0 has dimensions of particle density. These solutions are illustrated in Fig. 3, where we can see that the relative number of photoexcited excitons saturates to 1 slowly as a function of the temperature θ . The relative carrier number decreases with decreasing temperature as shown in Fig. 3(c).

Notice that the curve labeled P_T representing the product $\rho_e \rho_x$, which is proportional to the probability to form a trion, is as sizable as the fraction of the charge carriers below $\theta \sim 1$. In the following section we include explicitly the population of trions by finding the Saha equations that correspond to such case.

IV. PHOTONS IN EQUILIBRIUM WITH EXCITONS, TRIONS, ELECTRONS, AND HOLES

Figure 4 illustrates the presence of a residual attractive charge-dipole interaction between an exciton, i.e., a bound electron-hole pair, and a photoexcited quasiparticle (with strong polaronic character) in the conduction band. Under favorable conditions this interaction can lead to a bound state, which for simplicity we call a negatively charged excitonic

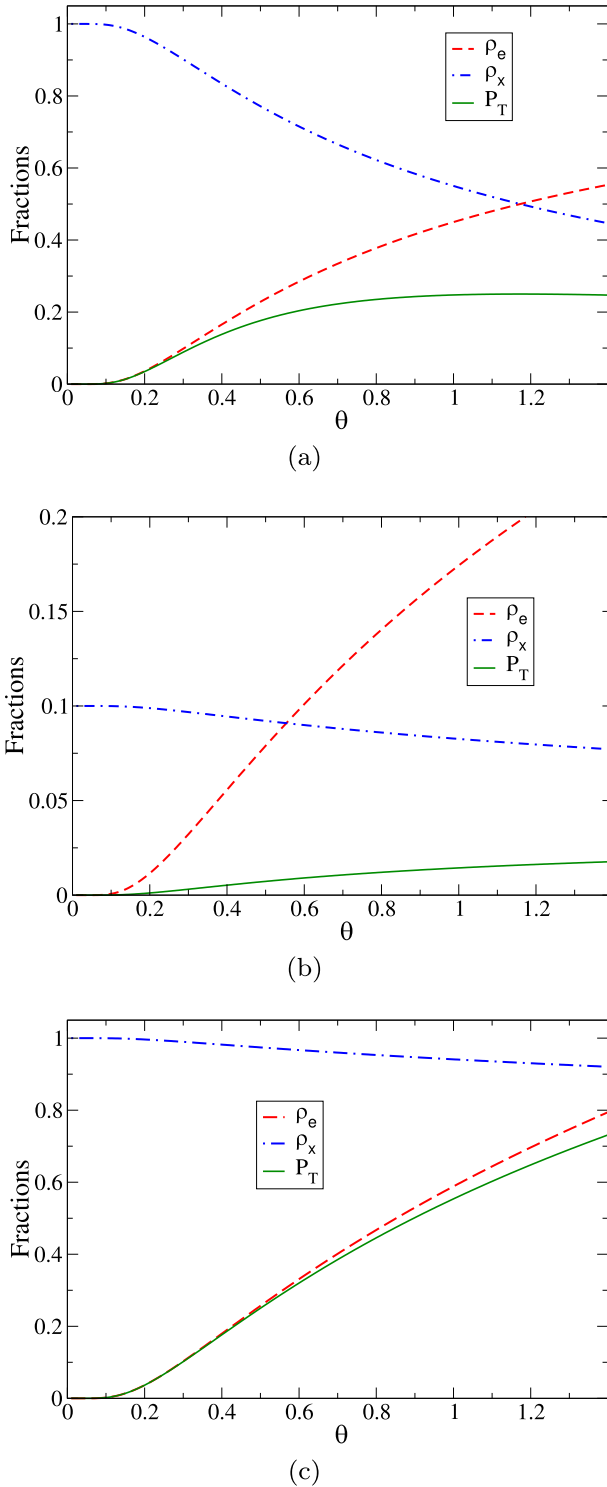


FIG. 3. Fractions of excitons, and electrons as a function of θ for (a) $m_e^* = m_x^* = 1$ and $\rho_p = 1$, (b) $m_e^* = m_x^* = 10$ and $\rho_p = 1$, and (c) $m_e^* = m_x^* = 10$ and $\rho_p = 10$.

trion. There is computational [28] and experimental [4,29] evidence that layered halide perovskites host such states and their binding energy is typically an order of magnitude smaller than that of excitons, i.e., in the tens of meV range [28]. When this state dissociates it dissociates to a polaron and a neutral exciton. It is expected to be quasistable for some time longer

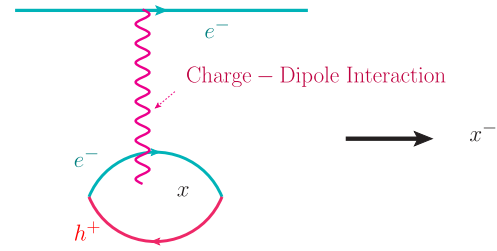


FIG. 4. A photoexcited exciton (x) (illustrated schematically as a bubble formed by a quiselectron and a quasihole propagator) with large binding energy in a semiconductor can attract a photoexcited quiselectron (of polaronlike character as illustrated in Fig. 1) via the charge-dipole interaction (illustrated as a magenta wiggly line) to form a trion (x^-). The trion binding energy is expected to be weaker by an order of magnitude compared to the exciton binding energy.

than the time required to reach quasiequilibrium with the rest of the carriers and excitons.

We will also assume that the recombination time is much longer [25,30,31] than the time required for the gas of these excitations, i.e., quiselectrons (e^-) and quasiholes (h^+), excitons (x) and excitonic trions (which we generically denote as x^- and x^+) to form a transient quasiequilibrium. When this quasiequilibrium is reached, let the area densities of these excitations be n_e, n_h, n_x, n_{x^-} and n_{x^+} , respectively.

We will also assume that initially every incident photon creates one electron/hole pair, a fraction of which rather quickly combine to form excitons (x) and charged excitonic trions (x^\pm). When quasiequilibrium is reached via the following processes,



the equilibrium densities are related to the photon density n_p as follows:

$$n_p = n_x + \frac{3}{2}(n_{x^-} + n_{x^+}) + \frac{1}{2}(n_e + n_h), \quad (16)$$

$$n_{x^-} + n_e = n_{x^+} + n_h, \quad (17)$$

where the last equation is the statement of charge neutrality. Equation (16) is obtained by assuming that every incident photon initially creates one electron/hole pair and at equilibrium n_{x^-} of the electrons combine with an equal number of neutral excitons to form n_{x^-} negatively charged excitonic trions while n_{x^+} of these initially photogenerated holes combine with an equal number of neutral excitons to form n_{x^+} of positively charged excitonic trions. Equation (16) is derived in the Appendix.

The object on the left-hand side (LHS) of each one of the above balance equations [Eqs. (13)–(15)] is a bound state of the two objects on the right-hand side (RHS) of the same equation, therefore, it has a lower energy. The excitation from the object on the LHS to that on the RHS and vice versa should satisfy a detailed balance. Equating the corresponding product of the equilibrium canonical distribution with the transition probability and that of the inverse process, at a common temperature T , leads to the following set of coupled Saha-type

equations:

$$\frac{r_e r_h}{r_x} = \sigma_0, \quad \frac{r_x r_e}{r_{x^-}} = \sigma_-, \quad \frac{r_x r_h}{r_{x^+}} = \sigma_+, \quad (18)$$

$$r_\lambda = \frac{n_\lambda}{m_\lambda^*}, \quad \lambda = x, x^-, x^+, e, h, \quad (19)$$

$$\sigma_\tau \equiv \frac{m_e k_B T}{\pi \hbar^2} e^{-|E_b^\pm|/k_B T}, \quad \tau = 0, \pm, \quad (20)$$

where $m_{x^\pm}^*$ is the effective mass (in units of the bare electron mass m_e) of the trions, and m_x^* , m_e^* , and m_h^* are the effective masses of the excitons, electrons, and holes. The area densities n_p , n_x , n_{x^-} , n_{x^+} , n_e , n_h have been defined earlier [after Eqs. (16) and (17)]. Here, E_b^\pm are the trion binding energies relative to the exciton binding energy.

Using the parameters θ and κ_0 introduced earlier, we can rewrite these equations as follows:

$$\frac{\rho_e \rho_h}{\rho_x} = \sigma_0(\theta), \quad \frac{\rho_x \rho_e}{\rho_{x^-}} = \sigma_-(\theta), \quad \frac{\rho_x \rho_h}{\rho_{x^+}} = \sigma_+(\theta), \quad (21)$$

$$\rho_\lambda = \frac{r_\lambda}{\kappa_0}, \quad \sigma_\pm(\theta) \equiv \theta e^{-\alpha^\pm/\theta}, \quad \alpha_\pm = \frac{E_b^\pm}{E_b^0}, \quad (22)$$

which should satisfy Eqs. (16) and (17), i.e.,

$$\rho_p = \left[m_x^* + \frac{3}{2}(\xi_- + \xi_+) \right] \frac{\rho_e \rho_h}{\sigma_0} + \frac{m_e^* \rho_e + m_h^* \rho_h}{2}, \quad (23)$$

$$(\xi_- - \xi_+) \rho_e \rho_h = \sigma_0(m_h^* \rho_h - m_e^* \rho_e), \quad (24)$$

where

$$\xi_- = \frac{m_{x^-}^* \rho_e}{\sigma_-}, \quad \xi_+ = \frac{m_{x^+}^* \rho_h}{\sigma_+}. \quad (25)$$

Equations (23) and (24) can be solved in terms of ρ_e and ρ_h , where the reduced photon density ρ_p and the effective masses are taken as input parameters. After obtaining these two densities, the excitonic and trionic densities are found using Eqs. (21).

In order to see the qualitative behavior of the solution to the above equations, we take the case where $E_b^+ = E_b^-$ and $m_{x^+}^* = m_{x^-}^* = m_e = m_h^* = m_e^*$, which imply that $n_{x^-} = n_{x^+}$. In Fig. 5 (top) we plot the fractions of the various carriers as a function of T in units of E_b^0 (i.e., as a function of θ) for the case where $\alpha_\pm = 0.1$, using photon density $\rho_p = 1$ (in units of κ_0). Notice that the trionic density remains constant as the temperature is lowered and below some temperature scale of the order of E_b^\pm (which is an order of magnitude smaller than the excitonic binding energy E_b^0) the trionic density begins to drop. In Fig. 5 (middle) we plot the fractions of the various carriers as a function of θ for $\alpha_\pm = 0.1$, using $m_{x^+}^* = m_{x^-}^* = m_x^* = 10$, $m_e = m_h^* = m_e^* = 1$, and photon density $\rho_p = 1$. Note the significant reduction to both the excitonic and the trionic densities. However, if we increase the photon density to $\rho_p = 10$, the density of excitons and trions (Fig. 5, bottom) increases to their initial values (i.e., Fig. 5, top).

To understand these values in physical units, ρ_p is in units of $\kappa_0 \simeq 7 \times 10^5 \mu\text{m}^{-2}$ and when the incident light is green and is under solar illumination fluences, which are orders of magnitude lower excitation fluences than in most spectroscopic measurements, the photon density per unit time is 2.5×10^9 photons/ $(\mu\text{m}^2 \text{s})$. The photocarrier decay times in well-passivated perovskites have been reported to be as long

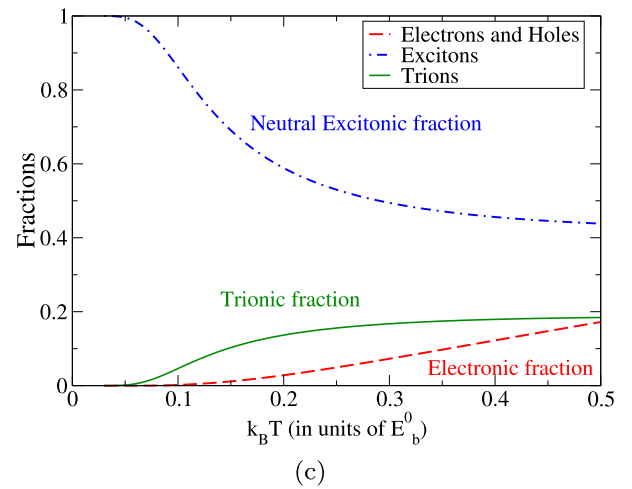
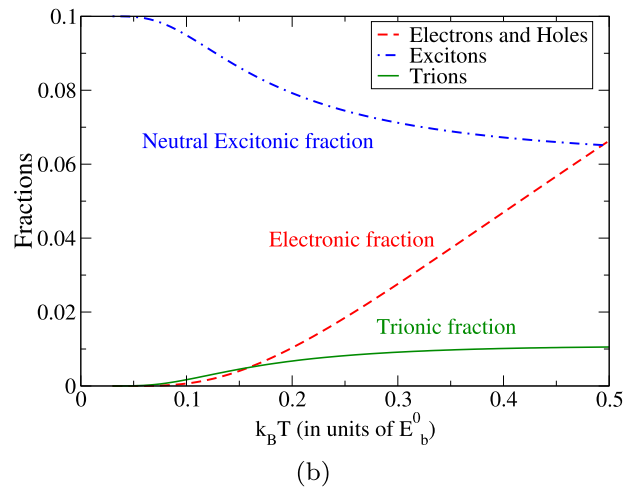
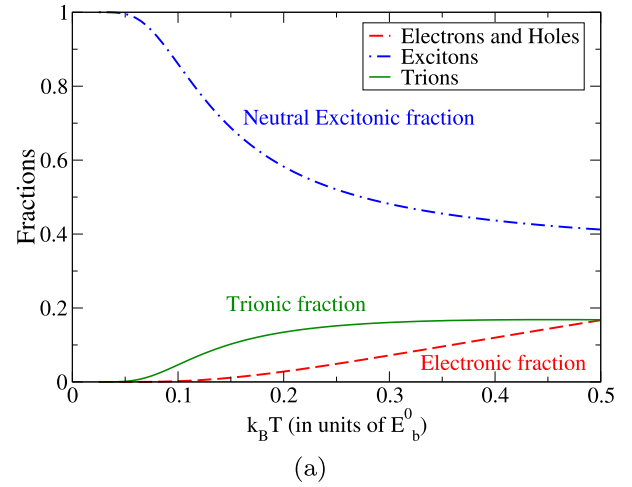


FIG. 5. Temperature dependence of the fractions of the various components for the case of $m_e^* = m_h^* = m_x^* = m_{x^-}^* = m_{x^+}^*$ and $\rho_p = 1$ (a); $m_e^* = m_h^* = 1$, $m_x^* = m_{x^-}^* = m_{x^+}^* = 10$, and $\rho_p = 1$ (b); and $m_e^* = m_h^* = 1$, $m_x^* = m_{x^-}^* = m_{x^+}^* = 10m_e^*$, and $\rho_p = 10$ (c).

as 10 μs , as measured by both photoluminescence and microwave conductivity [30,31]. This implies that in units of κ_0 , the average total carrier density is $\rho_p \sim 0.03$. Therefore, the values of $\rho_p = 1, 10$ used in Fig. 5 should be in the range of

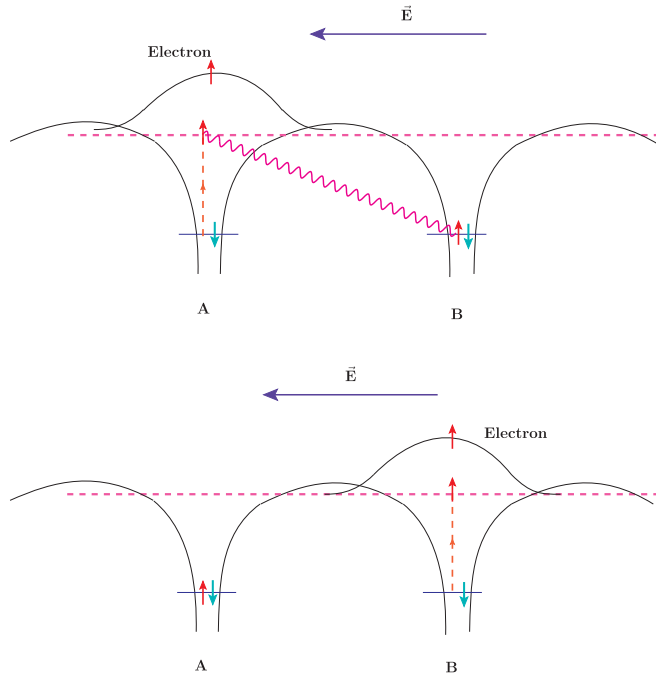


FIG. 6. Top: A third electron (schematically shown by the wavefunction envelope with an up-spin electron occupying it in site A) bound to an exciton (schematically illustrated in real space by the red arrow indicating that the up electron was promoted to an excited Wannier orbital) forming a trion. For ordinary trion tunneling to occur to a nearest-neighboring site, simultaneous energy transfer through the Coulomb interaction (magenta wiggly line) and electron transfer to a nearest-neighboring atomic site is required. Bottom: When these requirements are simultaneously met, the electron (and, thus, the trion) transfers to that nearest-neighbor site.

typical excitation fluences used in the reported spectroscopic measurements.

V. TRION TUNNELING

Figure 6 illustrates that an electrically charged excitonic state (a trion) in the presence of an external electric field could tunnel from one atomic site to a nearest-neighboring atomic site. This quantum-mechanical tunneling process is enabled by the energy offset between neighboring sites, which is caused by the presence of the electric field, \vec{E} , that lowers the energy of neighbor sites by an amount $-e\vec{E} \cdot \delta\vec{R}$ (where $\delta\vec{R}$ is the difference between the Bravais lattice vectors of two neighboring sites). This particular trion-tunneling mechanism requires a combined process to occur. First, the energy of the excited exciton, i.e., the bound electron/hole pair at the original site (to which the additional charge is bound), is transferred to the nearest-neighbor site by means of the electron-electron interaction (magenta wiggly line in Fig. 6), thereby creating a neutral exciton there. Simultaneously, the additional third electron bound to the trion x^- follows under the influence of the external electric field. Because this is a coherent combination of two processes, it is proportional to the product of the amplitude for the energy transfer and the tunneling amplitude for the electron to follow.

Notice that simultaneous energy and charge transfer is necessary to obtain hopping of a trion from one site to its

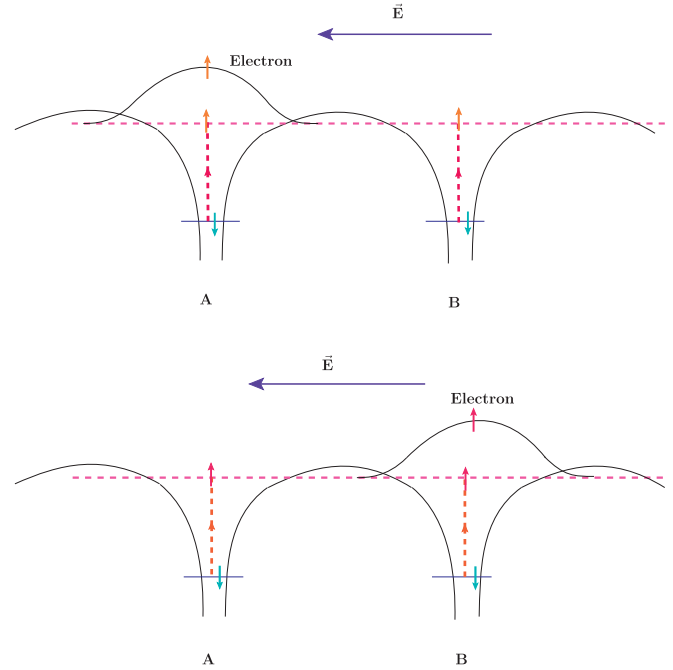


FIG. 7. Top: Since the neutral-exciton density can be very high at room temperature and below (Fig. 5), there is a significant probability that the third electron (schematically shown by the wavefunction envelope with the up-spin electron occupying it in site A) bound to an exciton (schematically illustrated in real space by the red arrow indicating that the up electron was promoted to an excited Wannier orbital) forming a trion to find a neutral exciton next to it in site B. Bottom: This will allow trion tunneling to such neighboring site by only charge (electron) hopping to site B producing the state shown in the bottom figure.

nearest neighbor (Fig. 6). However, there is the possibility that the neighboring site to a trion is occupied by an exciton (Fig. 7). As we have shown, the neutral exciton density (depending on the illumination fluences and recombination rate) can be high at or below room temperature (for room temperature $k_B T \ll E_b^0$, because the exciton binding energy E_b^0 is 0.35 eV), therefore, this becomes probable. In this case, the tunneling process in the presence of an exciton next to a trion, as illustrated in Fig. 7, requires only charge transfer without energy transfer, which can become more likely than the case of Fig. 6. A very similar process can take place which leads to the tunneling of x^+ trions. By means of such processes, trions of positive charge x^+ , i.e., bound states of an exciton with a photoexcited hole, under the influence of an external electric field will tunnel in the opposite direction and be collected by the opposite polarity lead.

Therefore, there is a quantum-mechanical mechanism for trion transfer, which does not fall into the semiclassical mechanism of electrical transport and could play a role in the photoconductivity mechanism in these materials.

VI. DISCUSSION AND CONCLUSIONS

In Sec. II we have discussed the nature of the elementary quasiparticles as well as that of composite quasiparticles which are expected to be photogenerated in 2D halide perovskites.

The relative populations of excitonic complexes which contain neutral excitons (x) as well as negatively (x^-) and positively (x^+) charged excitonic trions in quasiequilibrium with the photoexcited electron-hole pairs as a function of temperature T were studied in the limit where the binding energy for x excitons is a significant fraction of 1 eV and that for x^\pm is of the order of tens of meV. The Saha equations are derived for this multicomponent system of assumed long-lived photoexcitations in equilibrium with an incident photon gas of fixed area density n_p . This is a well-defined problem of statistical physics of very little, if any, ambiguity. In addition to the above-mentioned energy scales, the only other parameters entering the problem are the effective masses of the components of the system and n_p .

The solution to this problem reveals that as a function of temperature at room temperature and below for a wide range of values of the above-mentioned effective masses, for sufficiently high values of n_p , the trionic population is the dominant charge excitation of this system.

These findings, in conjunction with recent experimental evidence for their presence, the behavior and mobility of such excitonic trions in 2D hybrid perovskites [4,29], can explain the observed seemingly contradictory behavior of these materials, namely, that despite their large excitonic binding energy, there are plenty of charge carriers.

In this paper, it is also speculated in Sec. V that, when there is an applied external electric field, there are two different mechanisms of trion hopping to a nearest-neighbor site. One is a spontaneous process involving both energy and charge transfer and a second is a hopping process stimulated by a high neutral-exciton population, which is expected to be the case at or below room temperature (when the incident-light fluences are high enough), in which case trion tunneling is mediated by a nearest-neighbor neutral exciton. This speculation can help explain the observed sizable trion mobility [4,29], despite their complex structure, and leads to a novel transport mechanism in these materials. Excitonic trions were recently invoked to explain quantum beating phenomena in bulk perovskites [32] and in applications of time-resolved spectroscopic techniques to quantum dots [33] and colloidal nanocrystals [34] of cesium-lead halide as well as in attempts to analyze the excitation fluences dependence of transient absorption signals in CsPbBr₃ [35].

At a timescale where recombination occurs, it is reasonable to expect that these excitonic complexes, both the neutral and the charged excitons, will decay into photons and give rise to photoluminescence.

The role of biexcitons [36–38] can also be taken into consideration by extending the present approach. However, we tried to minimize the number of parameters involved in the present study for clarity. We do expect biexcitons to contribute with a somewhat sizable population at and below room temperature by depleting the exciton population by a very small fraction. However, we have no reason to expect that their inclusion would alter the qualitative results of our study regarding the relative populations of the charged excitations, i.e., trions and electron/hole pairs.

Finally, the scenario and an extension of the model of the role of trions discussed here, and in particular the Saha equations, which describe the quasiequilibrium of a fluid of

photoexcitations (i.e., unbound quasielectron/quasihole pairs, excitons, and trions) may be applicable to other materials. In particular, we expect this work to find application in transition metal dichalcogenides, where observations that these materials host exciton and trions with large binding energy have already been reported [39–42].

ACKNOWLEDGMENTS

The author thanks Hanwei Gao and Peng Xiong for useful discussions and for sharing their photoconductivity measurements prior to publication. This work was supported by the U.S. National Science Foundation under Grant No. NSF-EPM-2110814.

APPENDIX: DERIVATION OF RELATIONSHIP BETWEEN EXCITATION DENSITIES

In order to balance the number of absorbed photons per unit volume, n_p , we will break down the thought process as a three-level counting process. First, let us say that every absorbed photon creates an unbound electron/hole (e/h) pair, i.e.,

$$n_p = n_{e/h}^0. \quad (\text{A1})$$

However the number of unbound e/h pairs, i.e., $n_{e/h}^0$, is the same as the number of unbound electrons or the number of unbound holes, i.e., $n_{e/h}^0 = n_e^0 = n_h^0 = (n_e^0 + n_h^0)/2$, and in order to have a particle-hole symmetric equation, we can write

$$n_p = \frac{n_e^0 + n_h^0}{2}. \quad (\text{A2})$$

Next, we allow equilibrium between unbound e/h pairs and neutral excitons x , i.e., the process

$$x \longleftrightarrow e^- + h^+, \quad (\text{A3})$$

to take place. At the end of this process, a number δn_e^0 of electrons and an equal number of holes δn_h^0 ($\delta n_e^0 = \delta n_h^0$) will bind to form an equal number $n_x = \delta n_e^0 = \delta n_h^0$ of neutral excitons. The right-hand side of the above Eq. (A2) will be transformed as

$$n_p = n_x^{(1)} + \frac{n_e^{(1)} + n_h^{(1)}}{2}. \quad (\text{A4})$$

Namely, straightforward substitution of $n_e^{(1)} = n_e^0 - \delta n_e^0$, $n_h^{(1)} = n_h^0 - \delta n_h^0$, and $n_x^{(1)} = \delta n_e^0 = \delta n_h^0 = n_e^0 - \delta n_e^0$ in the above equation yields the originally assumed Eq. (A2).

In the third stage, we continue to keep the number of photons unchanged and by allowing the right-hand side of Eq. (A4) to change by using x 's, e 's, and h^+ 's to create x^- 's and x^+ 's, namely, the following equilibrium processes:

$$x^- \longleftrightarrow x + e^-, \quad (\text{A5})$$

$$x^+ \longleftrightarrow x + h^+. \quad (\text{A6})$$

Let us say $\delta n_x^{(1)}$ of the x 's are transformed to x^- 's to produce a number n_{x^-} of the latter, so that

$$\delta n_x^{(1)} = n_{x^-}. \quad (\text{A7})$$

However, they need to combine with $\delta n_e^{(1)}$ electrons from the $n_e^{(1)}$ electrons to do it. Therefore, they will reduce the number

of unbound electrons by

$$\delta n_e^{(1)} = \delta n_x^{(1)}, \quad (\text{A8})$$

and so the remaining electron density n_e will be given by

$$n_e = n_e^{(1)} - \delta n_e^{(1)} = n_e^{(1)} - \delta n_x^{(1)}. \quad (\text{A9})$$

Similarly, let us say another part $\delta n_x^{(2)}$ of the x 's is transformed to x^+ 's to produce a number of n_{x^+} of the latter, so that

$$\delta n_x^{(2)} = n_{x^+}. \quad (\text{A10})$$

These neutral excitons will need to combine with $\delta n_h^{(1)}$ holes from the $n_h^{(1)}$ holes to do it. Therefore, they will reduce the number of unbound holes by an amount of

$$\delta n_h^{(1)} = \delta n_x^{(2)}. \quad (\text{A11})$$

Hence, the remaining hole density n_h will be given by

$$n_h = n_h^{(1)} - \delta n_h^{(1)} = n_h^{(1)} - \delta n_x^{(2)}. \quad (\text{A12})$$

The right-hand side of Eq. (A4) is now written as

$$n_p = n_x + \delta n_x^{(1)} + \delta n_x^{(2)} + \frac{n_e + n_h}{2} + \frac{\delta n_e^{(1)} + \delta n_h^{(1)}}{2}. \quad (\text{A13})$$

Namely, we substituted in Eq. (A4) that $n_x^{(1)} = n_x + \delta n_x^{(1)} + \delta n_x^{(2)}$, $n_e^{(1)} = n_e + \delta n_e^{(1)}$, and $n_h^{(1)} = n_h + \delta n_h^{(1)}$.

Next, we substitute for $\delta n_e^{(1)}$ from Eq. (A8), and for $\delta n_h^{(1)}$ from Eq. (A11) to obtain

$$n_p = n_x + \delta n_x^{(1)} + \delta n_x^{(2)} + \frac{n_e + n_h}{2} + \frac{\delta n_x^{(1)} + \delta n_x^{(2)}}{2}, \quad (\text{A14})$$

which leads to

$$n_p = n_x + \frac{n_e + n_h}{2} + \frac{3(\delta n_x^{(1)} + \delta n_x^{(2)})}{2}. \quad (\text{A15})$$

We now use the fact that $\delta n_x^{(1)} = n_{x^-}$ [Eq. (A7)] and $\delta n_x^{(2)} = n_{x^+}$ [Eq. (A10)] to write

$$n_p = n_x + \frac{n_e + n_h}{2} + \frac{3(n_{x^-} + n_{x^+})}{2}, \quad (\text{A16})$$

which is Eq. (16) used in the main part of the paper.

Note that this final equation does not depend on the order of the various transformation processes. It simply expresses the pseudoparticle number conservation in these transformations.

-
- [1] C. C. Stoumpos, D. H. Cao, D. J. Clark, J. Young, J. M. Rondinelli, J. I. Jang, J. T. Hupp, and M. G. Kanatzidis, Ruddlesden–popper hybrid lead iodide perovskite 2D homologous semiconductors, *Chem. Mater.* **28**, 2852 (2016).
- [2] D. B. Mitzi, Synthesis, crystal structure, and optical and thermal properties of $(\text{C}_4\text{H}_9\text{NH}_3)_2\text{Ml}_4$ ($\text{M} = \text{Ge}, \text{Sn}, \text{Pb}$), *Chem. Mater.* **8**, 791 (1996).
- [3] X. Wu, M. T. Trinh, and X.-Y. Zhu, Excitonic many-body interactions in two-dimensional lead iodide perovskite quantum wells, *J. Phys. Chem. C* **119**, 14714 (2015).
- [4] J. D. Ziegler, Y. Cho, S. Terres, M. Menahem, T. Taniguchi, K. Watanabe, O. Yaffe, T. C. Berkelbach, and A. Chernikov, Mobile triions in electrically tunable 2D hybrid perovskites, *Adv. Mater.* **35**, 2210221 (2023).
- [5] J.-C. Blancon, H. Tsai, W. Nie, C. C. Stoumpos, L. Pedesseau, C. Katan, M. Kepenekian, C. M. M. Soe, K. Appavoo, M. Y. Sfeir, S. Tretiak, P. M. Ajayan, M. G. Kanatzidis, J. Even, J. J. Crochet, and A. D. Mohite, Extremely efficient internal exciton dissociation through edge states in layered 2D perovskites, *Science* **355**, 1288 (2017).
- [6] Y. Qin, Z.-G. Li, F.-F. Gao, H. Chen, X. Li, B. Xu, Q. Li, X. Jiang, W. Li, X. Wu, Z. Quan, L. Ye, Y. Zhang, Z. Lin, L. Pedesseau, J. Even, P. Lu, and X.-H. Bu, Dangling octahedra enable edge states in 2D lead halide perovskites, *Adv. Mater.* **34**, 2201666 (2022).
- [7] C. Zhao, W. Tian, J. Leng, Y. Zhao, and S. Jin, Controlling the property of edges in layered 2D perovskite single crystals, *J. Phys. Chem. Lett.* **10**, 3950 (2019).
- [8] Z. Zhang, W.-H. Fang, R. Long, and O. V. Prezhdo, Exciton dissociation and suppressed charge recombination at 2D perovskite edges: Key roles of unsaturated halide bonds and thermal disorder, *J. Am. Chem. Soc.* **141**, 15557 (2019).
- [9] A. R. Srimath Kandada and C. Silva, Exciton polarons in two-dimensional hybrid metal-halide perovskites, *J. Phys. Chem. Lett.* **11**, 3173 (2020).
- [10] J. Yin, H. Li, D. Cortecchia, C. Soci, and J.-L. Brédas, Excitonic and polaronic properties of 2D hybrid organic–inorganic perovskites, *ACS Energy Lett.* **2**, 417 (2017).
- [11] A. Simbula, R. Pau, Q. Wang, F. Liu, V. Sarritzu, S. Lai, M. Lodde, F. Mattana, G. Mula, A. Geddo Lehmann, I. D. Spanopoulos, M. G. Kanatzidis, D. Marongiu, F. Quochi, M. Saba, A. Mura, and G. Bongiovanni, Polaron plasma in equilibrium with bright excitons in 2D and 3D hybrid perovskites, *Adv. Opt. Mater.* **9**, 2100295 (2021).
- [12] B. Guzelturk, T. Winkler, T. W. J. Van de Goor, M. D. Smith, S. A. Bourelle, S. Feldmann, M. Trigo, S. W. Teitelbaum, H.-G. Steinrück, G. A. de la Pena, R. Alonso-Mori, D. Zhu, T. Sato, H. I. Karunadasa, M. F. Toney, F. Deschler, and A. M. Lindenberg, Visualization of dynamic polaronic strain fields in hybrid lead halide perovskites, *Nat. Mater.* **20**, 618 (2021).
- [13] K. Zheng, M. Abdellah, Q. Zhu, Q. Kong, G. Jennings, C. A. Kurtz, M. E. Messing, Y. Niu, D. J. Gosztola, M. J. Al-Marri, X. Zhang, T. Pullerits, and S. E. Canton, Direct experimental evidence for photoinduced strong-coupling polarons in organolead halide perovskite nanoparticles, *J. Phys. Chem. Lett.* **7**, 4535 (2016).
- [14] C. Liu, H. Tsai, W. Nie, D. J. Gosztola, and X. Zhang, Direct spectroscopic observation of the hole polaron in lead halide perovskites, *J. Phys. Chem. Lett.* **11**, 6256 (2020).
- [15] L. R. V. Buizza and L. M. Herz, Polarons and charge localization in metal-halide semiconductors for photovoltaic and light-emitting devices, *Adv. Mater.* **33**, 2007057 (2021).
- [16] W. Tao, Y. Zhang, and H. Zhu, Dynamic exciton polaron in two-dimensional lead halide perovskites and implications for optoelectronic applications, *Acc. Chem. Res.* **55**, 345 (2022).
- [17] C. Franchini, M. Reticioli, M. Setvin, and U. Diebold, Polarons in materials, *Nat. Rev. Mater.* **6**, 560 (2021).
- [18] A. Simbula, L. Wu, F. Pitzalis, R. Pau, S. Lai, F. Liu, S. Matta, D. Marongiu, F. Quochi, M. Saba, A. Mura, and G.

- Bongiovanni, Exciton dissociation in 2D layered metal-halide perovskites, *Nat. Commun.* **14**, 4125 (2023).
- [19] S. G. Motti, M. Kober-Czerny, M. Righetto, P. Holzhey, J. Smith, H. Kraus, H. J. Snaith, M. B. Johnston, and L. M. Herz, Exciton formation dynamics and band-like free charge-carrier transport in 2D metal halide perovskite semiconductors, *Adv. Funct. Mater.* **33**, 2300363 (2023).
- [20] F. Thouin, D. A. Valverde-Chávez, C. Quarti, D. Cortecchia, I. Bargigia, D. Beljonne, A. Petrozza, C. Silva, and A. R. Srimath Kandada, Phonon coherences reveal the polaronic character of excitons in two-dimensional lead halide perovskites, *Nat. Mater.* **18**, 349 (2019).
- [21] S. Das, J. E. Coulter, and E. Manousakis, Convergence of quasiparticle self-consistent *GW* calculations of transition-metal monoxides, *Phys. Rev. B* **91**, 115105 (2015).
- [22] J. E. Coulter, E. Manousakis, and A. Gali, Optoelectronic excitations and photovoltaic effect in strongly correlated materials, *Phys. Rev. B* **90**, 165142 (2014).
- [23] M. van Schilfgaarde, T. Kotani, and S. Faleev, Quasiparticle self-consistent *GW* theory, *Phys. Rev. Lett.* **96**, 226402 (2006).
- [24] M. Shishkin, M. Marsman, and G. Kresse, Accurate quasiparticle spectra from self-consistent *GW* calculations with vertex corrections, *Phys. Rev. Lett.* **99**, 246403 (2007).
- [25] D. W. deQuilettes, K. Frohna, D. Emin, T. Kirchartz, V. Bulovic, D. S. Ginger, and S. D. Stranks, Charge-carrier recombination in halide perovskites, *Chem. Rev.* **119**, 11007 (2019).
- [26] M. N. Saha, LIII. Ionization in the solar chromosphere, *Philos. Mag.* **40**, 472 (1920).
- [27] M. N. Saha and A. Fowler, On a physical theory of stellar spectra, *Proc. R. Soc. London Ser. A* **99**, 135 (1921).
- [28] Y. Cho, S. M. Greene, and T. C. Berkelbach, Simulations of trions and biexcitons in layered hybrid organic-inorganic lead halide perovskites, *Phys. Rev. Lett.* **126**, 216402 (2021).
- [29] Y. Kanemitsu, Trion dynamics in lead halide perovskite nanocrystals, *J. Chem. Phys.* **151**, 170902 (2019).
- [30] M. C. Brennan, S. Draguta, P. V. Kamat, and M. Kuno, Light-induced anion phase segregation in mixed halide perovskites, *ACS Energy Lett.* **3**, 204 (2018).
- [31] R. Brenes, D. Guo, A. Osherov, N. K. Noel, C. Eames, E. M. Hutter, S. K. Pathak, F. Niroui, R. H. Friend, M. S. Islam, H. J. Snaith, V. Bulović, T. J. Savenije, and S. D. Stranks, Metal halide perovskite polycrystalline films exhibiting properties of single crystals, *Joule* **1**, 155 (2017).
- [32] U. N. Huynh, Y. Liu, A. Chanana, D. R. Khanal, P. C. Sercel, J. Huang, and Z. V. Vardeny, Transient quantum beatings of trions in hybrid organic tri-iodine perovskite single crystal, *Nat. Commun.* **13**, 1428 (2022).
- [33] N. S. Makarov, S. Guo, O. Isaienko, W. Liu, I. Robel, and V. I. Klimov, Spectral and dynamical properties of single excitons, biexcitons, and trions in cesium-lead-halide perovskite quantum dots, *Nano Lett.* **16**, 2349 (2016).
- [34] G. Rainò, G. Nedelcu, L. Protesescu, M. I. Bodnarchuk, M. V. Kovalenko, R. F. Mahrt, and T. Stöferle, Single cesium lead halide perovskite nanocrystals at low temperature: Fast single-photon emission, reduced blinking, and exciton fine structure, *ACS Nano* **10**, 2485 (2016).
- [35] S. Nakahara, H. Tahara, G. Yumoto, T. Kawawaki, M. Saruyama, R. Sato, T. Teranishi, and Y. Kanemitsu, Suppression of trion formation in CsPbBr₃ perovskite nanocrystals by post-synthetic surface modification, *J. Phys. Chem. C* **122**, 22188 (2018).
- [36] F. Thouin, S. Neutzner, D. Cortecchia, V. A. Dragomir, C. Soci, T. Salim, Y. M. Lam, R. Leonelli, A. Petrozza, Ajay Ram Srimath Kandada, and C. Silva, Stable biexcitons in two-dimensional metal-halide perovskites with strong dynamic lattice disorder, *Phys. Rev. Mater.* **2**, 034001 (2018).
- [37] R. Su, C. Diederichs, J. Wang, T. C. H. Liew, J. Zhao, S. Liu, W. Xu, Z. Chen, and Q. Xiong, Room-temperature polariton lasing in all-inorganic perovskite nanoplatelets, *Nano Lett.* **17**, 3982 (2017).
- [38] E. P. Booker, M. B. Price, P. J. Budden, H. Abolins, Y. del Valle-Inclan Redondo, L. Eyre, I. Nasrallah, R. T. Phillips, R. H. Friend, F. Deschler, and N. C. Greenham, Vertical cavity biexciton lasing in 2D dodecylammonium lead iodide perovskites, *Adv. Opt. Mater.* **6**, 1800616 (2018).
- [39] Z. Li, T. Wang, Z. Lu, C. Jin, Y. Chen, Y. Meng, Z. Lian, T. Taniguchi, K. Watanabe, S. Zhang, D. Smirnov, and S.-F. Shi, Revealing the biexciton and trion-exciton complexes in BN encapsulated WSe₂, *Nat. Commun.* **9**, 3719 (2018).
- [40] M. Van der Donck, M. Zarenia, and F. M. Peeters, Excitons, trions, and biexcitons in transition-metal dichalcogenides: Magnetic-field dependence, *Phys. Rev. B* **97**, 195408 (2018).
- [41] S. Zhao, X. Huang, R. Gillen, Z. Li, S. Liu, K. Watanabe, T. Taniguchi, J. Maultzsch, J. Hone, A. Högele, and A. S. Baimuratov, Hybrid moiré excitons and trions in twisted MoTe₂-MoSe₂ heterobilayers, *Nano Lett.* **24**, 4917 (2024).
- [42] W. Chen, C. Zheng, J. Pei, and H. Zhan, External field regulation strategies for exciton dynamics in 2D TMDs, *Opt. Mater. Express* **13**, 1007 (2023).